Support Information

Computational methods

All density-functional theory (DFT) calculations were performed using the Gaussian 16 software package [1]. The molecular structure was visualized and all bond lengths and bond angles were measured by GaussView 6.0. Molecular orbitals were visualized by VMD [2]. All geometrical configurations were optimized using the M06-2X [3] hybrid function and Grimme D3 dispersion correction (GD3) [4], and the Def2-SVP [5] basis set was used for all atoms. Self-consistent calculations were performed using the M06-2X hybrid function and the Grimme D3 dispersion correction (GD3) and the Def2-TZVPP [6] basis set, with the addition of a diffusion function. The bond dissociation energy (BDE) is calculated in this paper using the following equation:

$$BDE = E_A + E_B - E_{AB}$$

where E_{AB} is the electronic energy of the complete structure before bond breaking, E_A and E_B are the electronic energies of the two radical fragments after bond breaking, respectively. In order to avoid wrongly incorporating the deformation energy of the fragments into the estimation of the bond strength, the two radical fragments are directly calculated by self-consistency without optimization.

In this paper, we use Multiwfn [7] to calculate the fuzzy bond order (FBO) [8] between F/O atoms and C radical of ether, the electrostatic potential (ESP) [9] of the C atom and the atomic dipole moment corrected Hirshfeld population atomic charge (AC) [10] of the C atom. NBO 7.0 [11] was used to derive the value of Second-order stabilization energy ($E^{(2)}$) between the lone pair electrons orbitals of the O/F atoms and the orbitals of the C radical, the O/F lone pair electrons orbital population number.

In this work, we use 5 regression models, Partial Least Squares Regression (PLS), Gradient Boosting Regression (GBR), Gaussian Process Regression (GPR), Support Vector Regression (SVR), Kernel Ridge Regression (KRR), to predict the antioxidative property of ether-based electrolytes. Each model was trained individually. 35 % of the samples in the dataset were randomly selected as test set, while the remaining samples

were used as training set. Moreover, we conduct a cross-validation combined with gridsearch approach to train the regression model and optimize the hyper-parameters (By utilizing the class sklearn.model_selection, Grid-SearchCV from Scikit-learn Python library (ver. 3.11.3)). In each fold, a fresh model is instantiated according to the previously defined model type and hyper-parameter combination, and then this model is trained using the training data for the current fold. After obtaining the optimal hyper-parameters, the model performance was assessed separately on the entire training set and the test set using these hyper-parameters. The detailed hyper-parameters used in this study can be found in Table S2.

Table S1 Optimized hyper-parameters of models used in this study (hyper-parameters not mentioned in the table are default values).

Model	Hyper-parameter
Partial Least Squares Regression (PLS)	n_components = 5
Gradient Boosting Regression (GBR)	learning_rate = 0.4 max_depth = 3 n_estimators = 100
Gaussian Process Regression (GPR)	n_restarts_optimizer = 0 random_state = 0
Support Vector Regression (SVR)	kernel = rbf C = 100 gamma = 0.1 epsilon = .1
Kernel Ridge Regression (KRR)	kernel = poly

	alpha = 0.5 coef0 = 4 gamma = 0.1

Table S2 The detailed description of 17 features and 2 target values

1	the change value of lone pair electrons population number of O1
2	the change value of lone pair electrons population number of O2
3	the total change value of lone pair electrons population number of O atoms adjacent to C1 (1 + 2)
4	the value of FBO between F atom and C1 radical
5	the change value of FBO between C1 radical and O1
6	the change value of FBO between C1 radical and O2
7	the total change value of FBO between C1 radical and the adjacent O atoms (5 + 6)
8	the total change value in lone pair electrons population number of O atoms adjacent to C2
9	the total change value of FBO between C2 radical and the adjacent O atoms
10	bond angles between F-C1-O1
11	bond angles between F-C1-O2
12	bond angles between F-C1-H
13	bond length of the C1-H bond
14	the value of BDE of C-H bond on ether carbons before substitution
15	the change value of ESP on C1
16	the change value of AC on C1
17	the change value of AC on C2
18	the change value of BDE of C-H bond on C1 (target value)
19	the change value of BDE of C-H bond on C2 (target value)

Table S3 The applicable situation of the five machine learning models

Model	Applicable situation	Relational expression
PLS (Partial Least Squares Regression)	linear combination relationships	The target variable can be expressed as a linear combination of key molecular descriptors:$y=\beta 1x1+\beta 2x2+\cdots+\beta nxn+\epsilon$
GBR (Gradient Boosting Regression)	higher-order interactions	The target variable is influenced by conditional-dependent nonlinear combinations of multiple descriptors
GPR (Gaussian Process Regression	uncertainty-driven complex relationships	The target variable is affected by latent variables or exhibits high noise levels
KRR (Kernel Ridge Regression)	continuous nonlinear relationships	There is a smooth and continuous nonlinear trend between the target variable and the descriptor
SVR (Support Vector Regression)	high-dimensional sparse nonlinear relationships	The target variable is dominated by a few critical descriptors in localized regions, resulting in piecewise nonlinear patterns

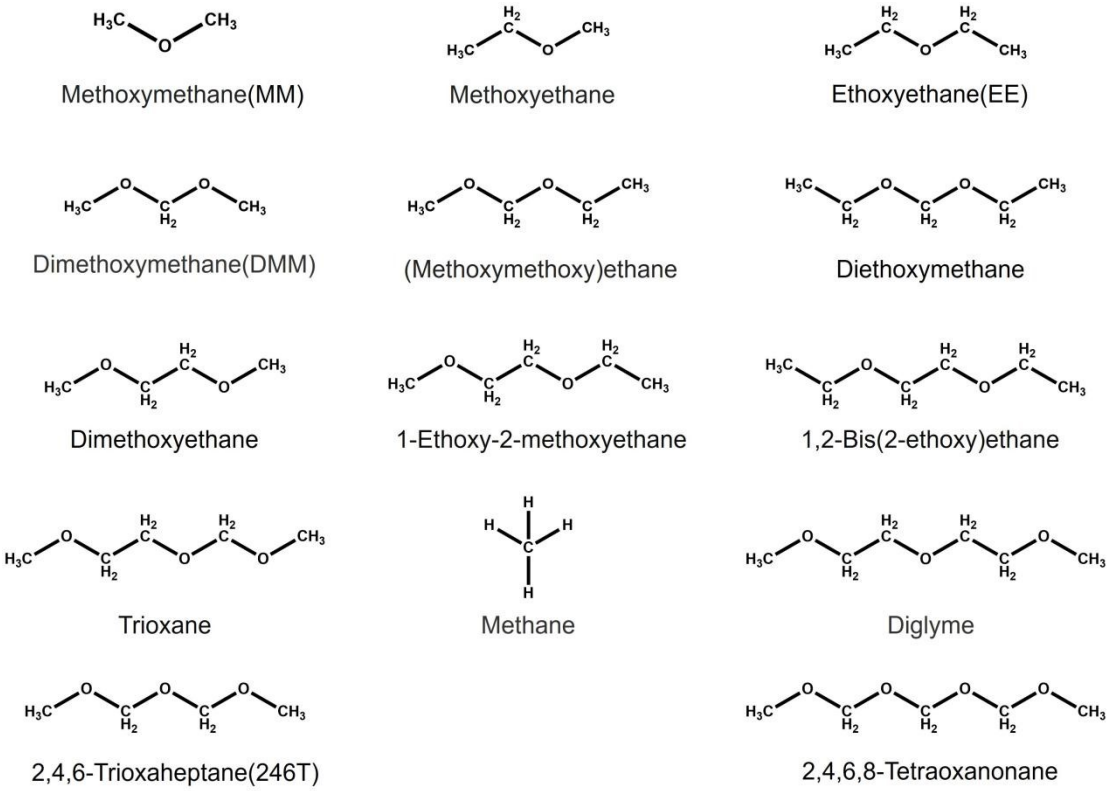

Figure S1 Structural formulae of molecules involved in the analysis

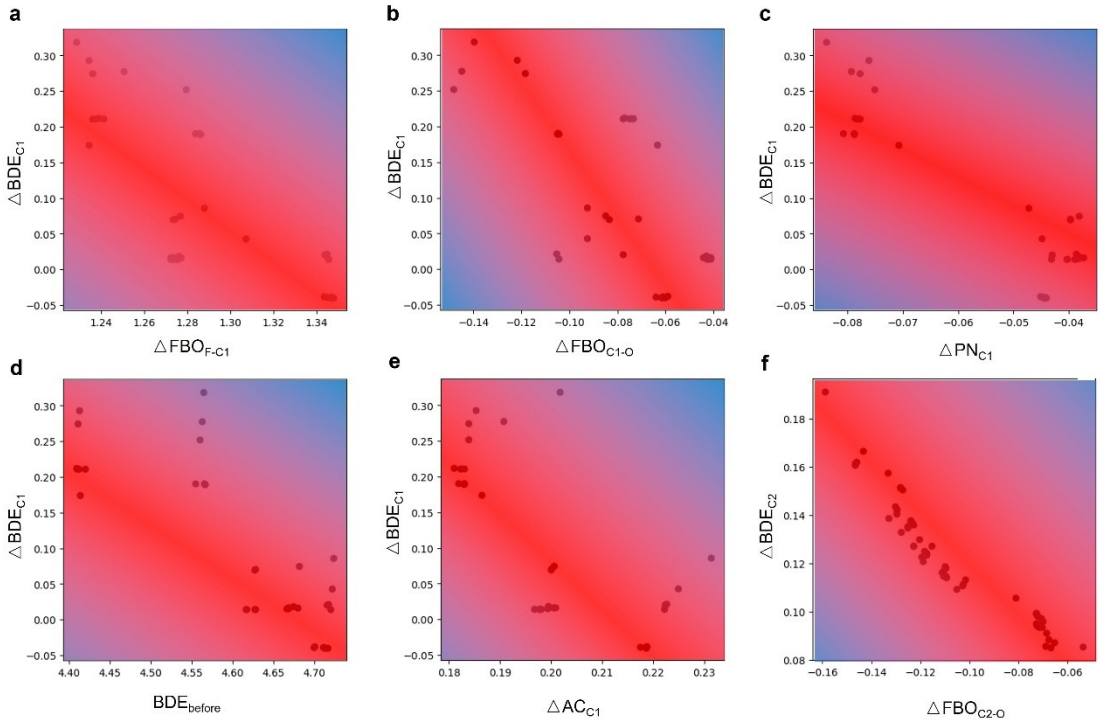

Figure S2 Scatter plots of the variation of ΔBDE_{C1} with (a) $FBO_{F\text{-}C1}$, (b) $\Delta FBO_{C1\text{-}O}$, (c) ΔPN_{C1}, (d) BDE_{before}, and (e) ΔAC_{C1}; (f) Scatter plot of the variation of ΔBDE_{C2} with $\Delta FBO_{C2\text{-}O}$.

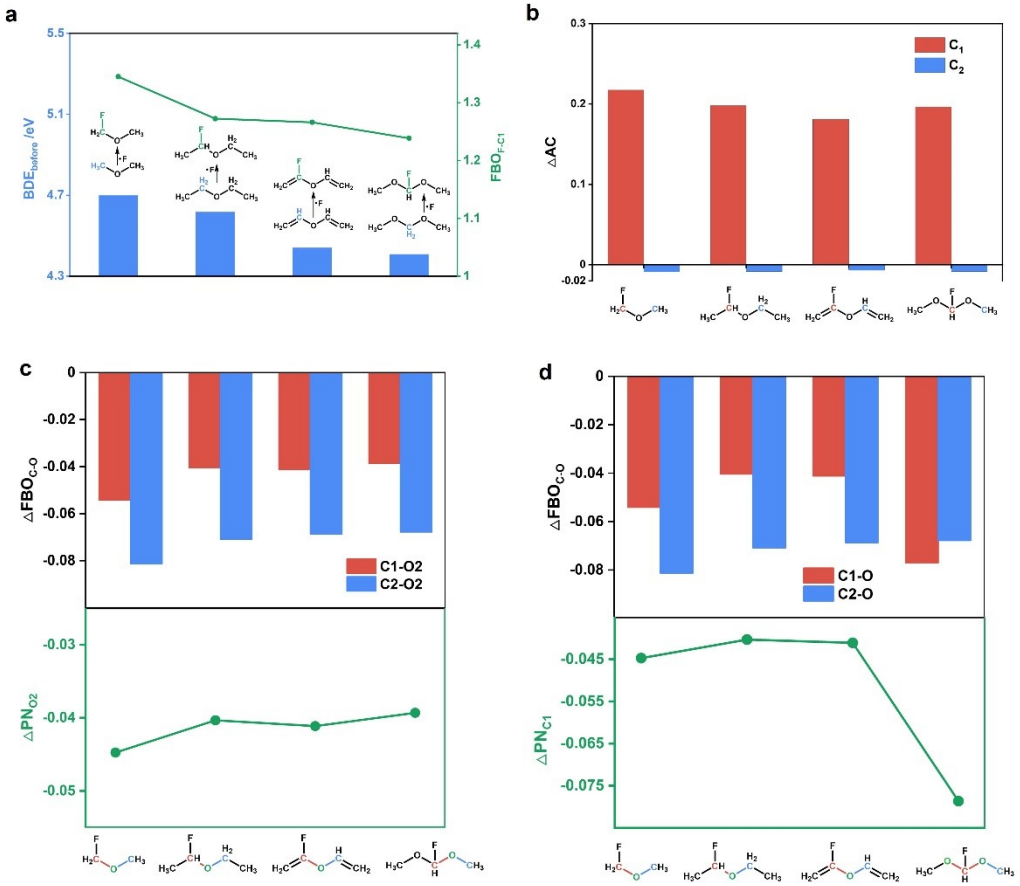

Figure S3 (a) BDE_{before} and $FBO_{F\text{-}C1}$ of Methoxymethane (MM), Ethoxyethane (EE), Allyl ether (AE), and Dimethoxymethane (DMM) (from left to right); (b) ΔAC of C atoms of MM, EE, AE, DMM; (c) ΔPN_{O2} and $\Delta FBO_{C\text{-}O}$ of MM, EE, AE, DMM; (d) ΔPN_{C1} and $\Delta FBO_{C\text{-}O}$ of MM, EE, AE, DMM.

Note S1

In Figure S3, the BDE_{before} gradually decreases with the variation of functional groups on the ether carbon from left to right. Thus, the stability of the C radical before substitution gradually increases with the variation. After substitution, the F atom and the C1 radical have the large FBO values, which indicates that F atom have a strong conjugation effect with C1 radical. ΔPN_{O2}, $\Delta FBO_{C1\text{-}O2}$, and $\Delta FBO_{C2\text{-}O2}$ are all less than 0. It indicates that after substitution, the number of local lone pair electrons of O2, the conjugation effect between the C1 radical and the O2, the conjugation effect between the C2 radical and the O2 all decrease. ΔPN_{C1}, $\Delta FBO_{C1\text{-}O}$, and $\Delta FBO_{C2\text{-}O}$ is also the case. ΔAC_{C1} value exceeds 0, indicating that after substitution, the positive charge

carried by C1 rises and the electron density of C1 decreases. $\triangle AC_{C2}$ changes very little, indicating that the electron density of C2 changes very little. With the variation of functional groups on the ether carbon, the $FBO_{F\text{-}C1}$ shows a trend of gradual decrease. However, ΔPN_{O2}, $\Delta FBO_{C1\text{-}O2}$, $\Delta FBO_{C2\text{-}O2}$, ΔAC_{C1} and ΔAC_{C2} show no significant changes with the variation of functional groups on the ether carbon. It is important to highlight that the ΔPN_{C1} and $\Delta FBO_{C1\text{-}O}$ of DMM are substantially smaller than that of the other three ethers. $\Delta FBO_{C2\text{-}O}$ still show no significant changes with the variation of functional groups on the ether carbon. This indicates that the two O atoms adjacent to C1 in DMM are both affected.

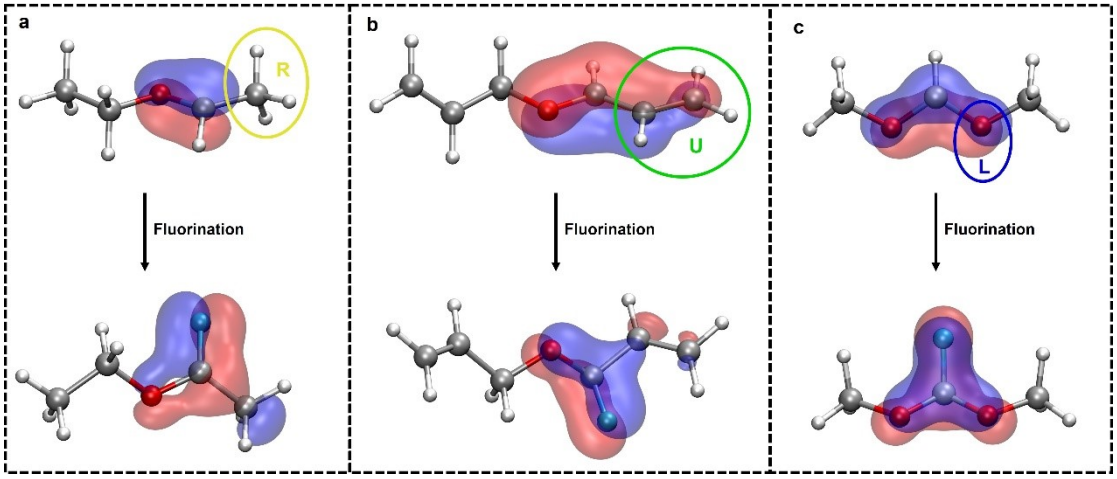

Figure S4 The molecular orbital images of (a) Ethoxyethane (EE); (b) Allyl ether (AE), and (c) Dimethoxymethane (DMM)

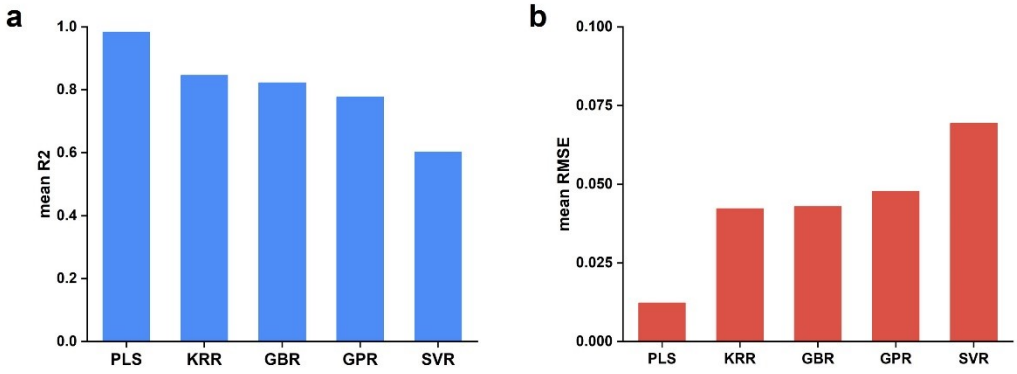

Figure S5 (a) mean R2, (b) mean RMSE for PLS, GBR, GPR, SVR, KRR models

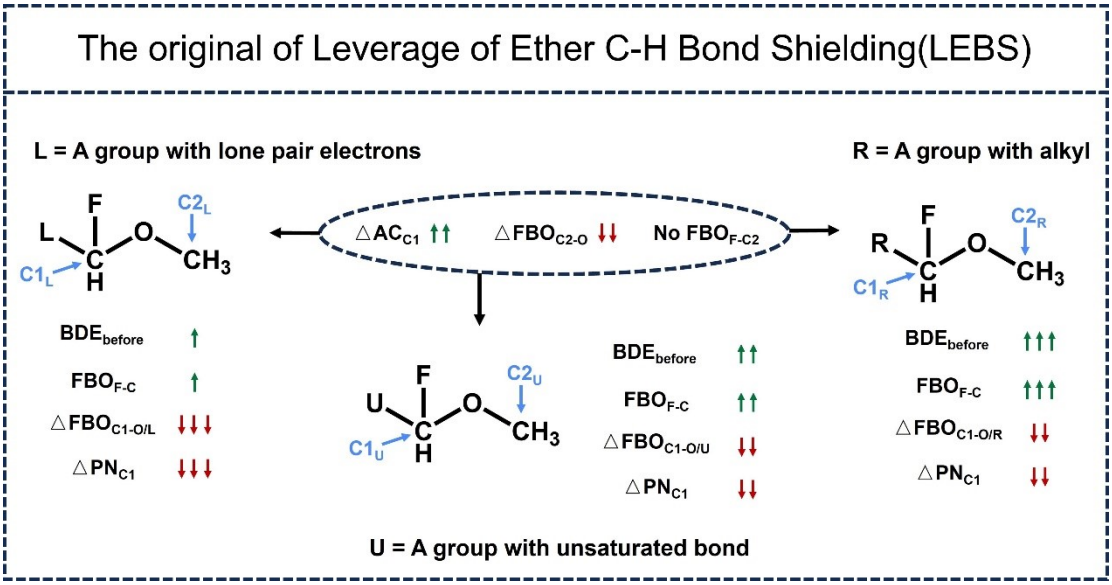

Figure S6 Schematic of the magnitude of various features for three types of ethers

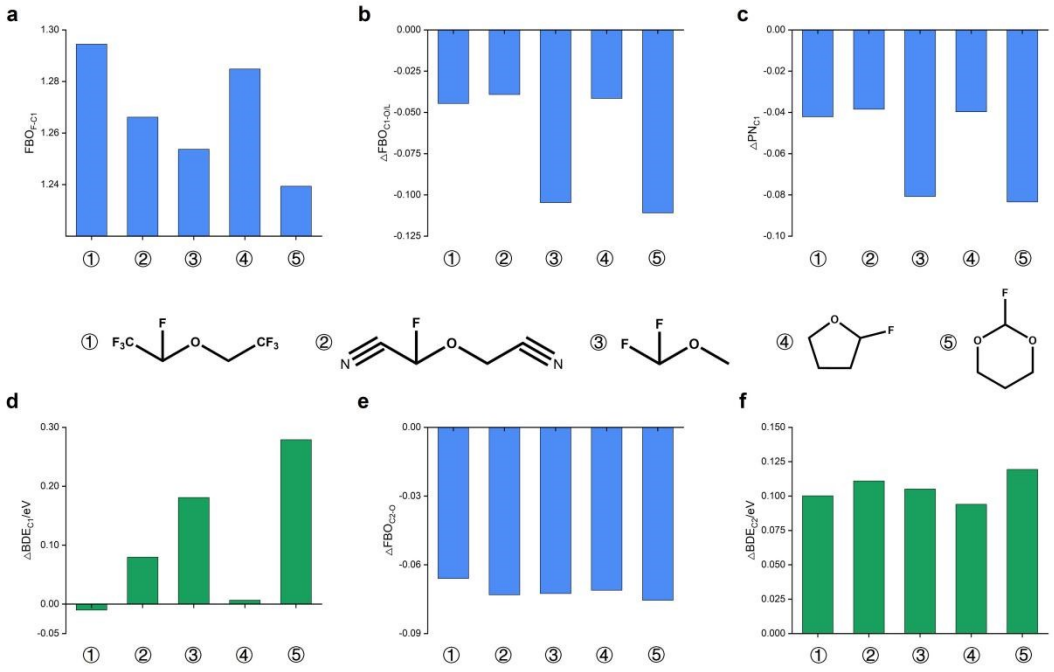

Figure S7 (a) FBO$_{F-C1}$, (b) △FBO$_{C1-O/L}$, (c) △PN$_{C1}$, (d) △BDE$_{C1}$, (e) △FBO$_{C2-O}$, (f) △BDE$_{C2}$ of ① Bis(2,2,2-trifluoroethyl) Ether, ② Dicyanomethoxyethane, ③ Fluoromethylmethylether, ④ Tetrahydrofuran, ⑤ 1,3- Dioxane after substitution

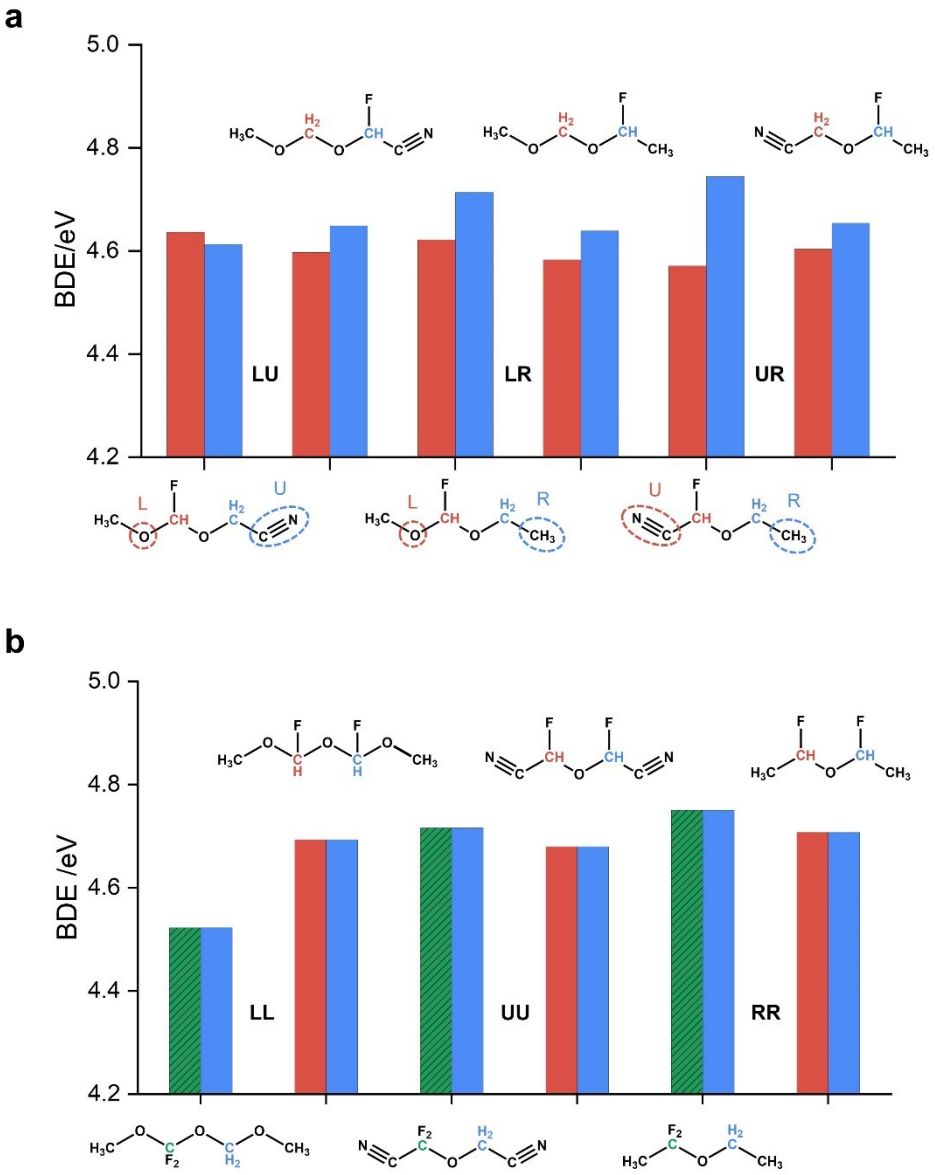

Figure S8 (a) BDE of the C-H bonds on two ether carbons after substitution by F in LU, LR, and UR type ethers; (b) BDE of the C-H bonds on two ether carbons after substitution in LL, UU, and RR type ethers (the BDE values of the C-H bonds on the two ether carbons correspond to the colors in the legend, with green stripes indicating no hydrogen on that C atom).

Note S2

To reflect the overall antioxidative property of the ether molecule after substitution, we should focus on the smaller BDE on two ether carbons after substitution. In the Figure S7, ether molecules of different types have been substituted through two distinct methods. We need to compare the two substitution methods within

the same ether molecule, focusing on the magnitude of the smaller BDE value on the two carbon atoms after substitution. Taking LU type ethers as an example, we need to compare the U-side (blue) BDE of the first substitution method with the L-side (red) BDE of the second substitution method. The results indicate that the BDE of the first substitution method is greater, suggesting a stronger overall antioxidative property.

References

[1] M. Frisch, G. Trucks, H. Schlegel, G. Scuseria, M. Robb, J. Cheeseman, G. Scalmani, V. Barone, G. Petersson, H. Nakatsuji, *Gaussian16 (Revision A. 03)* **2016**.

[2] W. Humphrey, A. Dalke, K. Schulten, *Journal of molecular graphics* **1996**, *14*, 33-38.

[3] Y. Zhao, D. G. Truhlar, *Theoretical chemistry accounts* **2008**, *120*, 215-241.

[4] S. Grimme, J. Antony, S. Ehrlich, H. Krieg, *The Journal of chemical physics* **2010**, *132*.

[5] F. Weigend, R. Ahlrichs, *Physical Chemistry Chemical Physics* **2005**, *7*, 3297-3305.

[6] D. M. Camaioni, C. A. Schwerdtfeger, *The Journal of Physical Chemistry A* **2005**, *109*, 10795-10797.

[7] T. Lu, F. Chen, *Journal of computational chemistry* **2012**, *33*, 580-592.

[8] I. Mayer, P. Salvador, *Chemical Physics Letters* **2004**, *383*, 368-375.

[9] a)J. S. Murray, P. Politzer, *Encyclopedia of computational chemistry* **2002**, *2*; b)J. S. Murray, P. Politzer, *Wiley Interdisciplinary Reviews: Computational Molecular Science* **2011**, *1*, 153-163.

[10] F. L. Hirshfeld, *Theoretica chimica acta* **1977**, *44*, 129-138.

[11] E. D. Glendening, C. R. Landis, F. Weinhold, *Journal of computational chemistry* **2019**, *40*, 2234-2241.